Deglacial evolution of regional Antarctic climate and Southern Ocean conditions in transient climate simulations

Daniel P. Lowry[1], Nicholas R. Golledge[1,2], Laurie Menviel[3,4], Nancy A.N. Bertler[1,2]

[1]Antarctic Research Centre, Victoria University of Wellington, Wellington, 6012, New Zealand
[2]GNS Science, Lower Hutt, 5010, New Zealand
[3]Climate Change Research Centre and PANGEA Research Centre, University of New South Wales, New South Wales, 2052, Australia
[4]ARC Centre of Excellence for Climate System Science, New South Wales, Sydney, Australia

Correspondence to: Daniel P. Lowry (Dan.Lowry@vuw.ac.nz)

Abstract. Constraining Antarctica's climate evolution since the end of the Last Glacial Maximum (~18kyr) remains a key challenge, but is important for accurately projecting future changes in Antarctic ice sheet mass balance. Here we perform spatial and temporal analysis of two transient deglacial climate simulations, one using a fully coupled GCM and one using an intermediate complexity model, to (1) better understand the mechanisms driving regional differences observed in paleoclimate records, and (2) identify the main strengths and limitations of the models in terms of parameters that impact ice sheet mass balance. The climate simulations show the greatest continental surface warming over the continental margins and regions with the greatest decrease in ice surface elevation, suggesting that sea ice-albedo feedbacks and ice sheet dynamics likely played strong roles in driving regional surface temperature differences during the deglaciation. The spatial distributions of simulated accumulation changes are quite distinct, with the intermediate complexity model experiencing resolution-related bias along the East Antarctic coast. Accumulation-temperature scaling relationships are fairly linear and constant further inland, but exhibit higher variability in the early to mid-Holocene over coastal regions. This climatic shift in the Holocene coincides with a weakening of the Amundsen Sea Low and a reduction in sea ice coverage. Circum-Antarctic coastal ocean temperatures at grounding line depths are highly sensitive to the meltwater forcings prescribed in each simulation, which are applied in different ways due to limited paleo-constraints. Although modelled centennial-scale rates of temperature and accumulation change are reasonable, clear model-proxy mismatches are observed with regard to the timing and duration of the Antarctic Cold Reversal (ACR) and Younger Dryas/early Holocene warming, suggesting that the Meltwater Pulse 1A and 1B events may be inadequately represented in these simulations. The incorporation of dynamic ice sheet models in future transient climate simulations could aid in improving meltwater forcing representation, and thus model-proxy agreement, through this time interval.

1. Introduction

Ice sheet model simulations of both past and future climates often rely on paleoclimate forcings derived from a combination of proxy data and climate model simulations (Pollard and DeConto, 2009; Golledge et al., 2014; Gregoire et al., 2016; Bakker et al., 2017). As such, the long memory of ice sheets with respect to past climatic conditions means that a model spin-up with an accurate deglacial climate forcing is important for any future Antarctic ice sheet model simulations. However, paleoclimate proxy data generally have sparse spatial coverage and relatively large uncertainties. Regional differences also persist in many of the Antarctic ice core

records due to local climate effects (Pedro et al., 2011; Veres et al., 2013), complicating their use as climate

50   forcings for an entire ice sheet. In addition to the ice core record, the marine proxy record is limited in aiding ice
sheet modellers due to the corrosive nature of Southern Ocean bottom waters, which inhibits the preservation of
microfossils that can be dated to provide age controls or geochemically analysed to provide a proxy for ocean
temperature (McKay et al., 2016). Although climate forcings derived from compilations of multiple records and
global datasets can help alleviate some of these issues, the regional differences between proxy archives may

55   actually be consequential to ice sheet mass changes (Golledge et al., 2017). For example, the Antarctic ice sheet
retreat during the last deglaciation likely occurred asynchronously (The RAISED Consortium, 2014), suggesting
that different sectors of the ice sheet responded either to different forcings, or in different ways to uniform
forcings.

Climate model simulations can help address the data gaps in the proxy record, however, they are often

60   assessed in terms of skill during climate states of relative stability, such as the Last Glacial Maximum (LGM),
the mid-Holocene or the Last Millennium (Bracconot et al., 2012; Schmidt et al., 2012; Hargreaves et al., 2013;
Sueyoshi et al., 2013), rather than over long-term periods of dramatic climate change. In fact, for the last
deglaciation, only one series of transient climate simulations using a fully coupled atmosphere-ocean general
circulation model (GCM) has been performed (Liu et al., 2009; He, 2011; He et al., 2013), and it may miss

65   important synoptic-scale processes related to the surface mass balance of West Antarctica (Fudge et al., 2016). It
also shows some discrepancies related to the timing and magnitude of the Antarctic Cold Reversal (ACR; He,
2011). Given that the task of simulating global climate with a variety of evolving internal and external forcings
is computationally demanding, the use of intermediate complexity models is especially appealing, and such
models have been successfully applied to better understand past climate changes (Menviel et al., 2011; Goosse

70   et al., 2012; Menviel et al., 2014). However, the coarser resolution and relatively simpler parameterization
schemes of the atmospheric models may introduce further challenges with regard to simulating the climatic
processes that affect ice sheet mass balance.

In this study, we evaluate the output of two transient deglacial climate simulations, one using a fully
coupled GCM (Liu et al., 2009) and one using an Earth system model of intermediate complexity (Menviel et

75   al., 2011). Given that the mass balance of the West and East Antarctic ice sheets is largely controlled by the
accumulation of snow on the surface minus the ice that is lost through sublimation, iceberg calving, sub-ice
shelf melt and thermal erosion of marine-based grounded ice, we focus on the aspects of climate that are most
relevant to these processes, including surface temperature, surface mass balance, ocean temperatures to
grounding line depths and sea ice. This analysis is performed in the context of the Antarctic ice core and

80   Southern Ocean marine sediment records. The main goals of this study are to (1) determine the regional
differences in the deglacial climate evolution of Antarctica and the Southern Ocean as recorded in the models
and proxy records, and (2) identify the main strengths and biases of the models in capturing the rates and
magnitudes of climatic changes that impact ice sheet mass balance. We focus our analysis on the period from
the last glacial termination (18 kyr; Denton et al., 2010) to the mid-Holocene (6.5 kyr).

85

2. Materials and Methods

2.1 Transient climate model simulations

90   In this study, we consider two transient deglacial climate simulations, namely, the TraCE-21ka and
LOVECLIM DG$_{ns}$ deglacial experiments (Table 1). TraCE-21ka is a transient climate simulation of the last
22,000 years using the Community Climate System Model version T31x3 (CCSM3), a synchronously coupled
GCM with atmosphere, ocean, land surface and sea ice components and a dynamic global vegetation module
(Collins et al., 2006; Liu et al., 2009; He, 2011). The transient forcings included evolving orbital forcing

95   following Milankovich theory (Genthon et al., 1987), greenhouse gas concentrations (CO_2, CH_4, N_2O; Joos and
Spahni, 2008), ice sheet and paleogeography changes based on the ICE-5G reconstruction (Peltier, 2004), and
prescribed meltwater fluxes into the Atlantic, North Atlantic and Southern Oceans (see He, 2011).

The LOVECLIM DG$_{ns}$ experiment was performed with the intermediate complexity LOVECLIM
model version 1.1 (Driesschaert et al. 2007; Goosse et al. 2007), which includes a T21 quasi-geostrophic

100   atmosphere model, an ocean general circulation model, a dynamic/thermodynamic sea ice model as well as
ocean carbon cycle and terrestrial vegetation components (Menviel et al. 2011). The horizontal resolution of the
atmosphere component is coarser than that of TraCE-21ka (T21 compared to T31), with 3 levels in the
atmosphere, but those of the ocean and sea ice components are similar (Table 1). The transient forcings included
time-varying solar insolation (Berger, 1978), Northern Hemisphere ice sheet topography updated every 100

105   years (Peltier, 1994), and atmospheric CO_2 determined from the EPICA Dome C ice core (Monnin et al. 2001),
with CH_4 and N_2O fixed at LGM levels. Freshwater pulses were applied to the North Atlantic and Southern
Ocean based on $^{231}Pa/^{230}Th$ data of the North Atlantic (McManus et al., 2004) and Greenland temperature
reconstructions (Alley, 2000). Two transient simulations were performed; one with freshwater input in the
Southern Ocean at the time of the ACR, and one without; we consider the former (see Menviel et al., 2011). We

110   also note that the ice sheet topography over Antarctica was unchanged in this simulation. Additional model
details of TraCE-21ka and LOVECLIM are presented in Table 1.

In terms of the transient forcings, one of the most uncertain aspects concerns the timing, magnitude and
location of meltwater fluxes, which are handled in the two simulations in different ways. In the early part of the
study period (18-14.5 kyr), a prescribed freshwater flux into the North Atlantic in TraCE-21ka is increased to

115   ~0.17 Sv, at which point it is held constant until 14.67 kyr. DG$_{ns}$ likewise has a prescribed freshwater flux into
the North Atlantic during this time interval, however the flux ceases earlier than in TraCE-21ka (0.2 Sv from
18-17.4 kyr; 0.25 Sv from 17.4 to 15.6 kyr). Meltwater Pulse 1A (MWP1A) is also represented differently: in
TraCE-21ka, very high, short-lived freshwater fluxes into the Ross and Weddell Seas occur between 14.35 and
13.85, peaking at ~14.1 kyr (0.33 Sv each), with lower freshwater forcing applied to the Mackenzie River and

120   Gulf of Mexico regions (reaching 0.11 Sv each). In contrast, in DG$_{ns}$ a higher freshwater flux is applied in the
North Atlantic as compared to those in the Ross and Weddell Seas (0.2-0.25 Sv vs. 0.15 Sv, linearly decreasing
to 0 Sv, respectively), and the meltwater forcing occurs over a longer duration than in TraCE-21ka (14.4 to 13.0
kyr). For the Younger Dryas, an Arctic Ocean meltwater forcing is applied from 13-12.2 kyr in DG$_{ns}$ (0.25 Sv),
whereas in TraCE-21ka, a lower meltwater forcing is applied in the mid-latitude St. Lawrence River region from

125   12.9 to 11.7 kyr (0.17 Sv). In the Holocene, TraCE-21ka has a large meltwater forcing of 5 Sv in the Hudson
Strait region at 8.47 kyr for half a year to represent the 8.2 ka event, but no such forcing is applied in DG$_{ns}$.
Additional details on the prescribed meltwater forcings in the DG$_{ns}$ and TraCE-21ka experiments can be found
in Menviel et al. (2011) and He (2011), respectively.

130   **2.2 Proxy Record**

The climate model simulations were compared with the temperature reconstructions of the Vostok (V; Lorius et al., 1995; Petit et al., 1999), Dome Fuji (DF; Uemura et al, 2012), and James Ross Island ice cores (JRI; Mulvaney et al., 2012), and the temperature and accumulation reconstructions of the EPICA Dome C (EDC; Jouzel et al., 2007; Parennin et al., 2007; Stenni et al., 2010) and West Antarctic Ice Sheet Divide ice cores (WDC; WAIS Divide Project Members, 2013; Cuffey et al., 2016; Fudge et al., 2016). See Figure 1 for ice core locations. Only publicly available Antarctic ice core records with temperature and/or accumulation reconstructions that overlapped with the period covered in both models (18-6.5 kyr) were used in this analysis. The exception is James Ross Island, which does not extend back to 18 kyr, hence only the period of 14.2 to 6.5 kyr is considered for this site.

The temperature reconstructions are commonly calculated as anomalies to modern temperatures based on deuterium (δD), deuterium excess (*d*) and oxygen isotope measurements (δO^{18}) using site-specific temperature-dependence relationships that assume the modern-day calibration holds over the entire record (Jouzel et al., 1997; Mulvaney et al., 2012). However, surface temperatures can also be more accurately determined with additional borehole temperature and nitrogen isotope data (Cuffey et al., 2016; Fudge et al., 2016). The accumulation reconstructions are more difficult to obtain, but can be estimated from the depth-age relationship by correcting the annual-layer thicknesses for flow-induced thinning using an ice flow model (Parennin et al., 2007; Fudge et al., 2016).

We also use a compilation of sea surface temperature (SST) records from the Southern Ocean. The records include alkenone-derived SST from Core MD03-2611 off the coast of South Australia (Calvo et al., 2007), Core TN057-21-PC2 in the South Atlantic (Sachs et al., 2001), and the Ocean Drilling Program (ODP) core of site 1233 off the coast of Southern Chile (Kaiser et al., 2005), and Mg/Ca-derived SST from Core MD97-2120 from Chatham Rise (Pahnke et al., 2003). Additional details on the proxy data are presented in Table 2.

2.3 Spatial and Temporal Analysis

We assess the magnitudes and rates of continental surface temperature and accumulation changes in both the climate simulations and ice core reconstructions from the start of the glacial termination (18kyr; Denton et al., 2010) to the mid-Holocene (6.5kyr), a period of time covered by both climate model simulations. Four continental regions are considered: the interior of the East Antarctic ice sheet (EAIS interior; 83°S-75°S, 30°W-165°E), coastal East Antarctica (coastal EAIS; 75°S-68°S, 15°W-165°E), West Antarctica (WAIS; 83°S-72°S, 165°E-30°W), and the Antarctic Peninsula (AP; 72°S-64°S, 64°W-59°W).

Here, we define accumulation as precipitation minus surface evaporation/sublimation (P – E). Accumulation from the ERA-Interim Analysis defined as precipitation minus sublimation has been shown to closely match airborne radar observations over the Thwaites Glacier in West Antarctica (Medley et al., 2013), however, we note that the contribution of wind-transported snow may also be locally significant in some areas, particularly in coastal areas dominated by katabatic winds (Palm et al., 2017). As such, we emphasize caution in interpreting accumulation changes in the climate models in areas of strong wind speed, but in terms of overall ice sheet mass balance, wind-transported snow is generally considered to be a relatively minor component (Palm et al., 2017). We also ignore the surface runoff term given that it is dependent on snow thickness thresholds that

are set in the climate models, hence over long timescales, it balances P-E over Antarctica. For each continental region, we determine the scaling relationships between temperature and accumulation in both climate model simulations and compare these relationships to those recorded in the ice core records. We also calculate the ratio of the 500 yr-change in annual average accumulation to the 500 yr-change in annual average surface temperature to explore how the temperature-precipitation relationships evolve through time.

In addition to continental surface temperature and accumulation, we examine changes in the surface ocean near the continental shelf to depths corresponding to modern-day grounding lines (0-800 m) as well as sea ice thickness, concentration and extent. Although we lack direct comparisons to sea ice thickness and Southern Ocean temperatures to 800 m depth in the marine proxy record, the changes observed in the climate model simulations are analyzed in the context of global and Southern Ocean SST and sea ice concentration reconstructions available for the period of 18 kyr to 6.5 kyr. Since the TraCE-21ka ocean and sea ice outputs are available at the decadal scale, and the ice core and marine sediment proxy record are also limited in temporal resolution, we focus this analysis on decadal- to centennial-scale changes.

3. Results

3.1 Surface temperature

The DG$_{ns}$ and TraCE-21ka deglacial simulations both show fairly uniform temperature increases over the continent and Southern Ocean of >6°C (Fig. 1a,b). The exception is the Antarctic Plateau and inland East Antarctica in the DG$_{ns}$ simulation, which exhibit more modest temperature increases, particularly closer to the pole. In contrast, the TraCE-21ka simulation experiences the greatest warming over the Antarctic Plateau (>10°C). This difference is primarily driven by the change in ice sheet topography in TraCE-21ka; the decrease in surface elevation can explain most of the temperature increase, as indicated by a sensitivity simulation in which only the ice sheet topography is changed while all other boundary conditions remain the same (Supplementary Information). Assuming a lapse rate of 1.0°C/100m, ~4-11°C of temperature change in the continental interior can be accounted for by topographic changes alone according to the ICE-5G estimations used in TraCE-21ka; if this lapse rate were applied to DG$_{ns}$, this would account for between ~50-100% of the temperature difference of the two model simulations in the inland region depending on the location. Both models simulate large temperature increases along the coasts over the Ross, Amundsen, and Bellingshausen Seas, as well as the West Pacific sector of East Antarctica (>10°C) due to decreases in annual average sea ice coverage. DG$_{ns}$ displays a larger temperature increase over the Antarctic Peninsula and Weddell Sea (10-13°C), whereas TraCE21ka shows a larger temperature increase at Prydz Bay (~12°C), primarily due to differences in modelled sea ice, which is discussed in greater detail below.

In terms of the overall surface temperature change from the glacial termination to the mid-Holocene, TraCE-21ka performs better with respect to the EAIS interior ice cores, with differences of 0.12°C, 0.50°C, and 1.98°C to the DF, EDC and V surface temperature reconstructions, respectively. For the first 4 kyr of the simulation, DG$_{ns}$ has a warm bias in the EAIS interior in terms of the temperature anomaly close to the pole due to its use of a modern Antarctic ice sheet configuration and model edge effects. TraCE-21ka has a cold bias for the full extent of the analyzed time period for WAIS and until ~9 kyr in the EAIS interior (Fig 1c,e). Although the site-specific modelled temperature change over WDC is underestimated in DG$_{ns}$ due to the above-mentioned topographic issue (Fig 1a), the wider WAIS regional average has a difference of <1.0°C with the WDC ice core

reconstruction (Fig 1e), as the more substantial warming along the coastal region compensates for this effect.

215 Over WAIS and the AP, TraCE-21ka overestimates the surface temperature increase relative to the WDC and JRI records (>3.0°C). Compared to the WDC ice core, TraCE-21ka underestimates the surface temperature change until a substantial increase occurs at 11.3 kyr due to an abrupt decrease in the ice surface elevation. This occurs at a time of stable temperature in the ice core record (Fig 1e). Both models show cold biases for the AP, but DG_{ns} converges with the JRI reconstruction in the early Holocene. Overall, the temperature anomalies are

220 more similar between the model simulations and ice cores in the Holocene than earlier in the deglacial period, with model-proxy differences within the range of the temperature proxy uncertainty. However, we note that some of the differences between the models and ice core temperature reconstructions could be due to local climate effects of the ice core sites that are not captured in the broad regional averages of the climate models.

In each region, the main discrepancy of the models with the Antarctic ice core temperature records is

225 the timing and magnitude of the ACR. The TraCE-21ka simulation displays a sharp ACR following a large pulse of freshwater into the Southern Ocean and the Gulf of Mexico, with a decrease in surface temperature of ~2.5°C in continental Antarctica, and a minimum occurring at approximately 14 kyr. The duration of the event is short-lived, lasting less than 500 years, as AMOC strength decreases back to its pre-meltwater forcing level (He, 2011). The ACR duration is longer in the DG_{ns} simulation (~1-1.5 kyr), initiating at approximately the

230 same time as in the TraCE21ka simulation, but the magnitude of the surface temperature change is lower, especially over the EAIS interior region (Fig 1c). In contrast to the simulations, the EAIS ice core records show a later initiation of the ACR, beginning at about 14 kyr, rather than peaking at this time. The WDC ice core exhibits a similar initiation timing to the climate model simulations, but shows a more gradual decrease and subsequent increase in temperature (Fig 1e). The overall surface temperature change of the ACR is moderate in

235 the ice core records as compared to the low (high) temperature change in DG_{ns} (TraCE21ka), and the event lasts for approximately 2 kyr, depending on the site. The JRI ice core shows the subtlest expression of the ACR, with the WDC, EDC and V ice cores displaying more pronounced signals.

3.2 Surface mass balance

240

Precipitation increases in every grid cell over the continent and Southern Ocean in the TraCE-21ka simulation over the period from 18 to 6.5 kyr, and these changes are significant at the 95% confidence level (Fig. 2a). The greatest increases occur over WAIS, coastal EAIS, and most of the Southern Ocean (>8 cm/yr). The AP, EAIS interior, and the Roosevelt Island region show modest increases (<4 cm/yr). The DG_{ns} simulation

245 shows a similar precipitation increase over the Southern Ocean (>8 cm/yr), however, precipitation decreases of 1-6 cm/yr occur over the pole and the coastal EAIS (Fig 2b). This is related to the coarse model resolution, which cannot adequately reproduce the steep slopes of East Antarctica and thus underestimates snow deposition in this region (Goosse et al., 2012). Also, in contrast to TraCE-21ka, DG_{ns} precipitation over the AP increases by >12 cm/yr, and increases by 4-10 cm/yr over the EAIS interior.

250

Modelled P-E anomalies relative to the preindustrial era (PI) are quite distinct in each region and differ to the accumulation reconstructions of the ice core records (Fig 2c-f). In general, the E term is substantially lower than the P term, hence E has a negligible effect on the surface mass budget. At 18 kyr, both models generally show negative P-E anomalies relative to PI. The exception is the coastal EAIS region in the DG_{ns} simulation, which shows higher relative P-E. The models show the highest P-E variability over the AP (Fig 2f).

255   In this region, TraCE-21ka remains near PI P-E levels, whereas DG$_{ns}$ shows a more substantial increase through time. The overall accumulation change at the WDC site for the analyzed period is similar to that of TraCE-21ka (Fig 2e), though the model has a negative P-E bias until the large ice sheet configuration change (decrease in surface elevation) that occurs at 11.3 kyr. Accumulation recorded in the EDC ice core is relatively stable. In fact, Cavitte et al. (2017) highlights the stability of accumulation patterns at Dome C over the last glacial cycle,

260   and the greatest change in the centennial-averaged record of annual average accumulation is only 2.17 cm/yr. TraCE-21ka shows a negative P-E anomaly relative to PI through this time interval, however, it exhibits a similar magnitude of change and variability in the deglacial period to the EDC accumulation record (Fig 2c). In contrast to TraCE-21ka, the DG$_{ns}$ simulation overestimates the magnitude and variability of P-E in the EAIS interior, and shows a negative trend though time along the EAIS coast (Fig 2d).

265

3.3 Accumulation-temperature relationships and rates of change

Centennial-scale rates of surface temperature and accumulation changes in the ice core records are well-matched by the climate model simulations, although the timing of the largest changes are generally offset

270   (Fig 3a-d). This is particularly true for surface temperature, with the ice core records generally showing warming (cooling) not exceeding 0.4°C (-0.2°C)/100 yrs and the climate models showing a slightly larger range (-0.5 to 0.6°C/100 years in the case of TraCE-21ka). The greatest discrepancies between the ice cores and the models are the timing and magnitude of cooling and warming associated with the ACR and an artificial warming spike in TraCE-21ka associated with the change in ice surface topography at 11.3 kyr. The DG$_{ns}$

275   simulation also shows a high warming rate following the ACR in each region, however, this is not due to any change in ice surface elevation. The models show similar variability in the precipitation changes (% relative to PI)/100yrs to those of the ice core accumulation records (Fig 3e-h). Of note is the increase and subsequent decrease in the accumulation rate that occurs following the ACR, which is present in both the WDC and EDC records, which slightly exceed the climate model precipitation rate variability. As expected, the models both

280   show substantially higher variability in the rate of precipitation change along the coasts.

In terms of the relationship between temperature and accumulation, Frieler et al., (2015) demonstrated that in 5 East Antarctic ice core records of the deglacial period, a consistent positive linear scaling relationship exists, with an average of ~6.0% °C^{-1}, in accordance with that expected of the Clausius Clapeyron relationship. The TraCE-21ka simulation captures these relationships at these individual sites relatively well, generally

285   falling within the range of uncertainty in the ice core record. Here, we show that the DG$_{ns}$ simulation using the intermediate complexity model can likewise reproduce this positive scaling relationship in the EAIS interior, however, the model fails in the coastal region of the EAIS (Fig 4a,b). This is explained by the model resolution issue mentioned previously, which is enhanced through time as the moisture gradient between the EAIS interior and the Southern Ocean is reduced.

290   In contrast to the EAIS ice cores, Fudge et al. (2016) highlighted the variability of the accumulation-temperature scaling relationship at the WDC site, noting three distinct periods in the 31 kyr record: an initial positive relationship from 31-15 kyr (5.7% °C^{-1}), a weak negative relationship from 15-8 kyr (-2.2% °C^{-1}), and a strong positive relationship from 8-0 kyr (17.0% °C^{-1}). This suggests that the WDC site experiences synoptic-scale variability in precipitation not present at the EAIS ice core locations, and also not reproduced by the

295   TraCE-21ka simulation. The DG$_{ns}$ simulation shows higher variability in accumulation as West Antarctic

temperatures approach near-PI levels in the mid-Holocene (Fig 4c). We have no accumulation record for the JRI site to compare with the models. However, both simulations exhibit similar behavior in the AP region, with a shift in the scaling relationship with warming temperatures (Fig 4d). TraCE-21ka shifts to a slight negative relationship, while DG_{ns} begins to show a weaker relationship with high variability, suggesting that the AP

300   region is also impacted by dynamical changes in the model simulations that counters the thermodynamic temperature scaling. In the case of TraCE-21ka, this circulation change reduces the amount of precipitation over this region.

We also examine the ratio of the 500 yr precipitation change to the 500 yr temperature change to explore how this relationship temporally evolves in the climate models. Since some of the Antarctic ice core
305   accumulation reconstructions are not fully independent from the temperature reconstructions (Veres et al., 2013; Frieler et al., 2015), analysis of the relationship cannot be performed for the ice cores except at multi-millennial timescales (Fudge et al., 2016), hence only the climate models are considered here. Figure 4e-h shows that the models remain nearly constant at the average scaling relationship, however, high variability occurs in the mid-Holocene in TraCE-21ka in the coastal regions, and to a lesser extent in DG_{ns}, suggesting a greater influence of
310   synoptic-scale processes in precipitation at this time. The onset of high variability in accumulation-temperature scaling occurs earlier in DG_{ns} over the AP than over the coastal EAIS, but it occurs synchronously over the two regions at ~9.5 kyr in TraCE-21ka (Fig 4h,f). The WAIS and EAIS regions exhibit comparatively less variability in the scaling relationship (Fig 4e,g), but the relationship is not constant in time for either region.

315   **3.4 Ocean temperatures and sea ice**

A composite of four Southern Ocean SST reconstructions shows an increase in SST from 18 to 6.5 kyr of 4.0°C (Fig 5a). The majority of warming occurs between 18 and 11 kyr, at which point SST decreases by ~1.0°C until 9.5 kyr, and remains stable into the mid-Holocene. The DG_{ns} experiment accurately simulates the
320   overall SST change for this period, but mismatches with the proxy record still occur, particularly with an overestimation of SST cooling with the ACR and an underestimation of SST warming in the early Holocene. The TraCE-21ka simulation underestimates SST changes throughout the time period, with an overall SST increase of 2.5°C. SST in TraCE-21ka also shows a pronounced decrease corresponding to the ACR. The ACR in TraCE-21ka also has a much shorter duration than that in DG_{ns}. Despite the strong link between AMOC and
325   mean ocean temperature, Bereiter et al., (2018) note a 700-yr ocean warming in the early Holocene, potentially associated with the drainage of Lake Agassiz, that cannot be fully reproduced by AMOC changes in GCM experiments. As such, this time period remains a challenge for both intermediate complexity models and GCMs, as demonstrated here.

At latitudes higher than 62°S, SSTs in both the TraCE-21ka and DG_{ns} simulations exhibit modest
330   warming, with similar increases in the Ross, Amundsen and Bellingshausen Seas (Fig. 5b-e). The DG_{ns} simulation shows greater sea surface warming in the Weddell Sea and the East Antarctic coastal seas (0.3-0.6°C). In the subsurface, TraCE-21ka initially shows much cooler temperatures during the LGM relative to PI. As a result, temperatures at 400 m depth increase by 2.1-2.7°C between 18 and 6.5 kyr. In comparison, the DG_{ns} simulation, which is much closer to its PI temperature at 18 kyr, shows relatively modest warming during the
335   simulation period.

Meltwater input in the Southern Ocean at the time of MWP1A decreases AABW formation and enhances the incursion of Circumpolar Deep Water on the Antarctic shelf in climate model simulations (Menviel et al., 2010), thus leading to a sub-surface warming along the Antarctic coasts. Following the different meltwater forcings used in the two models (see Methods), this sub-surface warming occurs earlier and for a

340 shorter duration in the TraCE-21ka than in DG_{ns}, with an offset of 1.2 kyr in the Weddell Sea. With the exception of this rapid warming event, the greatest amount of sub-surface warming in TraCE-21ka occurs between 11.5 and 9.5 kyr. In the Ross Sea, the warming continues into the Holocene in the layer between 250 and 800 m (Fig. 6). The DG_{ns} simulation shows little difference between SST and temperature at 400 m depth in this 64°S latitudinal band. An exception occurs during the ACR, where sub-surface temperatures increase, while

345 SSTs remain relatively unchanged as much of these coastal zones are covered in sea ice throughout the simulation period. The difference in surface and sub-surface temperatures is especially pronounced in the Indian and West Pacific Ocean sectors (Fig 6c,i). Greater warming occurs at depths below 500 m, however, this warming is still relatively minor compared to that observed in the TraCE-21ka simulation.

Both deglacial simulations show a substantial decrease in sea ice coverage, thickness and extent

350 (defined here as 5% coverage) between 18 and 6.5 kyr, interrupted only by an increase in sea ice in the Ross and Amundsen Seas during the ACR (Fig 7,8). In comparison to the LGM sea ice extent and concentration reconstructions (Gersonde et al., 2005), TraCE-21ka overestimates glacial sea ice extent at 18kyr in all ocean sectors; in fact, the TraCE-21ka 8 kyr sea ice extent better matches the LGM proxy record (Fig 7a). DG_{ns} sea ice extent at 18kyr matches the LGM record in the Indian Ocean sector, but underestimates (overestimates) sea ice

355 extent in the Atlantic (Pacific) sector (Fig 7b). Sea ice is generally thicker and has greater centennial-scale coverage in the TraCE-21ka simulation than in the DG_{ns} simulation, particularly in the Weddell Sea, where the thickest sea ice is found in both simulations (Fig 8). The greatest decrease in sea ice thickness also occurs in the Weddell Sea through time in both simulations, however, the decrease is much greater in TraCE-21ka.

360 **3.5 Southern Ocean-Antarctic Climate connections**

As described in section 3.1, the regions displaying the greatest increases in continental surface temperature that are not associated with changing ice sheet topography occur along the continental margins (Fig 1a,b), suggesting that albedo-driven radiative changes associated with sea ice coverage may be an important

365 driver of regional warming differences. Mean 100 yr-average sea ice coverage (%) decreases by 16, 20, and 21% in the TraCE-21ka simulation in the Ross Sea, the Amundsen and Bellingshausen Seas, and along the East Antarctic coast, respectively, but the Weddell Sea remains fully covered by sea ice through this interval (Fig 8a-d). Meanwhile, the DG_{ns} simulation shows decreases of 24, 21, 30, and 12% in these coastal regions, respectively. Changes in sea ice coverage may also explain the coastal warming differences observed between

370 DG_{ns} and TraCE-21ka. In particular, Oates Land, the West Antarctic coastal margin, and the Ronne ice shelf sector all show enhanced warming in the DG_{ns} simulation relative to that observed in TraCE-21ka (Fig 1a,b), as the difference in sea ice coverage of DG_{ns} relative to that of TraCE-21ka increases by 8% and 11% in the Ross and Weddell Seas, respectively.

In addition to linkages with continental temperatures, Southern Ocean conditions exert a strong

375 influence on Antarctic accumulation patterns (Delaygue, 2000; Stenni et al., 2010). Figures 9 and 10 show the Pearson linear cross-correlation coefficients (r) of linearly de-trended modelled decadal SST and precipitation

for 4 ice core locations in each continental region (i.e., WDC, EDC, JRI, and Law Dome (LD)) for DG$_{ns}$ and
TraCE-21ka, respectively. SSTs generally show strong spatial correlations to continental accumulation in both
models in the early deglacial period (18-12 kyr), however, these relationships weaken or become more negative

380 in the early to mid-Holocene (12-6.5 kyr). The difference in millennial-scale variability between the two
periods, which is higher in the early deglacial period, with Heinrich Stadial 1, the ACR, and Younger Dryas,
likely contributes to this shift in correlation strength. In addition, the retreat of sea ice extent and reduced annual
sea ice coverage in the early to mid-Holocene (Fig 7, Fig 8e-h) may also introduce a greater variety of moisture
sources of continental precipitation and alter the synoptic-scale variability, thereby weakening the SST-

385 precipitation correlations in both models. The correlations are higher for TraCE-21ka than DG$_{ns}$ at every site
except JRI, where the difference between the early deglacial period and early to mid-Holocene is starkest as the
correlations transition from positive to slightly negative (Fig 10g,h). The models both exhibit high positive
correlations between SSTs in the Indian and Pacific sectors with EDC precipitation in the early deglacial period
(18-12 kyr). Both models also show high positive correlations between WDC precipitation and SSTs in the

390 Pacific sector in the early deglacial period, but these correlations weaken in the Holocene, particularly in the
DG$_{ns}$ simulation (Fig 9c). Less model consistency exists at the coastal sites, most notably at LD (Fig 9c,d,
10c,d), which is likely related to the above-mentioned resolution limitation of DG$_{ns}$ along the EAIS coast.

To better understand the transitions in the accumulation relationships to continental temperatures and
SSTs in the early Holocene, we consider changes in 500hPa geopotential height anomalies over the Southern

395 Ocean and their relation to changes in atmospheric circulation. More specifically, the Amundsen Sea Low,
which is the largest influence on meridional circulation in the region, acts as a major control on the temperature
and precipitation in West Antarctica (Raphael et al., 2016). Modeling studies and ice core analyses have
suggested that atmospheric teleconnections driven by tropical SST anomalies in the Pacific trigger a quasi-
stationary wave response that reduces pressure over the Amundsen Sea. However, they offer conflicting

400 accounts of teleconnection strength during glacial conditions (Timmermann et al., 2010; Jones et al., 2018). At
18 kyr, the models display negative 500hPa geopotential height anomalies over much of the Southern Ocean
(Fig 11), in contrast to the LGM simulation of Jones et al., (2018), which shows positive anomalies over the
Amundsen Sea associated with a more El Niño-like state due to the orographic effects of the North American
ice sheet. The anomalies are more extreme in the TraCE-21ka than in DG$_{ns}$, particularly with regard to the

405 positive anomalies observed over the ice sheet, which is primarily driven by the ice sheet topographic changes.
Strong negative anomalies over the Amundsen Sea are observed in both models during the ACR (Fig 11c,j). A
deepened Amundsen Sea Low is generally associated with enhanced northerly flow across the AP, allowing for
intrusions of marine air masses over WAIS (Hosking et al., 2013). Through time, the simulated geopotential
height increases over the Southern Ocean to near-PI levels, reaching a state of reduced variance over the

410 Amundsen Sea in the early Holocene, consistent with the timing of reduced accumulation-temperature scaling
over the AP in both model simulations (Fig 4d).

4. Discussion

415 ### 4.1 Regional patterns of deglacial climate evolution

The deglacial model simulations and Antarctic ice core records demonstrate clear regional differences
between East and West Antarctica as well as between coastal regions and the continental interior in terms of

deglacial warming, driven primarily by oceanic influences. In comparison to the East Antarctic ice cores, the WDC isotope record indicates that the glacial termination of the more heavily marine-influenced WAIS initiated

420   ~2 kyr earlier than EAIS, with warming that reached near-mid Holocene levels by 15 kyr, coincident with a decline in circum-Antarctic sea ice (WAIS Divide Project Members, 2013; Cuffey et al., 2016). Although the climate models underestimate the rate of warming between 18-15 kyr over WDC, they do show greater warming rates for the WAIS, AP, and coastal EAIS regions, also occurring synchronously with the greatest declines in coastal sea ice, as compared to the less-marine influenced EAIS interior. The ice cores and models constrain

425   centennial-scale warming rates to within 0.6°C, with the most rapid warming occurring at the end of the ACR, excluding the abrupt ice mask-induced warming in TraCE-21ka. In terms of the spatial pattern of temperature change from the termination to the mid-Holocene, the greatest continental warming occurs over sea ice-adjacent land and areas of lowered ice surface elevation, highlighting the strong effects of albedo and orography on regional temperatures in Antarctica. The sea ice-albedo effect may be overestimated in the models over the AP,

430   as demonstrated by the JRI temperature reconstruction; however, Mulvaney et al. (2012) do note the strong sensitivity of AP temperature to ice shelf-related changes, with rapid warming events in the early Holocene and over the past 100 years (1.56 ± 0.42°C). Additional temperature and methane sulphonic acid reconstructions of coastal Antarctic ice cores could further elucidate the regional sensitivities to localized ice shelf and sea ice changes and identify possible thresholds.

435   In comparison to surface temperature, the regional evolution of accumulation and its relationship to surface temperature and conditions in the Southern Ocean through the deglacial period remain less clear. The two climate simulations show substantial differences with regard to the overall magnitude of accumulation changes in each region. In both the ice core records and the models, accumulation over the ice sheet generally shows higher variability in coastal regions, as expected, with the EAIS interior displaying consistent

440   temperature-accumulation scaling relationships at various sites, as previously demonstrated by Frieler et al. (2015). A primary limitation of the intermediate complexity LOVECLIM model is the inadequate resolution for the steep elevation gradient of the coastal EAIS, which leads to a precipitation bias in the region in the DG_{ns} simulation. This effect worsens through time due to the reduced moisture gradient between the Southern Ocean and the EAIS interior, as P-E increases over the EAIS interior, presumably from thermodynamic scaling with

445   temperature. The climate models show limited variability in accumulation-temperature scaling over WAIS, in contrast to the WDC record (Fudge et al., 2016); however, the AP exhibits a marked shift in the early to mid-Holocene, which may be due to changes in atmospheric circulation. This climatic shift in the early to mid-Holocene coincides with the reduced variance and weakening of the Amundsen Sea Low, which achieves near-present day conditions in both models by ~12 kyr. The weakened Amundsen Sea Low appears to reduce the

450   accumulation-temperature scaling over the AP in both models, and in the case of TraCE-21ka, a slight negative scaling relationship is observed; although this is not observed over the greater WAIS region, it should be noted that the timing is roughly consistent with the slight negative scaling period observed in the WDC record (15-8 kyr).

It may be expected that the retreat of sea ice and increased area of open ocean may introduce additional

455   moisture sources, thereby enhancing precipitation relative to temperature. In fact, coastal ice core records of the Holocene, including Taylor Dome, Law Dome, Siple Dome, have exhibited decoupling between accumulation and temperature that has been attributed to moist-air cyclonic activity and changes in sea ice conditions (Monnin

et al., 2004). Although the climate simulations do not exhibit a substantial increase in the scaling relationship

with reduced sea ice coverage, much higher temporal variability is observed over coastal EAIS in the mid-

460 Holocene. Likewise, the reduced correlations between Antarctic precipitation at the inland ice core locations and

SSTs in the Holocene may demonstrate that this effect is not limited to the coasts in these climate simulations.

The linkages between sea ice coverage, atmospheric dynamics and continental accumulation may also have

important implications for future projections of the more heavily marine-influenced WAIS climate, as GCMs

used in the Coupled Model Intercomparison Project 5 (CMIP5) tend to project higher accumulation-temperature

465 scaling in the future due to reduced sea ice coverage (Palerme et al., 2017). This effect may also be quite

regionally dependent, as no statistically significant increase has been observed over the Thwaites glacier over

the past three decades (Medley et al., 2013). The results here also highlight that dynamical processes cannot be

discounted in Antarctic accumulation projections. Additional moisture budget analysis is warranted to better

constrain the effects of circulation changes and cyclonic-driven precipitation on Antarctic accumulation in

470 transient climate simulations, particularly in relation to tropical and mid-latitude teleconnections with the

Amundsen Sea Low.

4.2 Transient climate modeling limitations and implications for Antarctic ice sheet modeling

475   Both transient simulations display discrepancies with the paleo-records across the ACR and early

Holocene. In the case of TraCE-21ka, the ACR is more abrupt and of a larger magnitude than in the ice core

temperature and SST reconstructions, which is related to how the MWP1A meltwater forcing is applied between

14.35 and 13.85 kyr (see Methods). He (2011) performed a sensitivity experiment with CCSM3, in which the

prescribed meltwater discharge in both hemispheres associated with MWP1A was excluded, that improves on

480 the ACR model-proxy agreement. The meltwater discharge applied to the North Atlantic prior to the ACR (17-

14.67 kyr) suppresses the upper cell of the AMOC. When this freshwater forcing is terminated at 14.67 kyr,

AMOC recovers. Without the inclusion of MWP1A meltwater discharge during the Bølling-Allerød interstadial,

Antarctic surface temperatures can remain cooler for a longer duration due to the bipolar seesaw response to the

rapid increase in AMOC strength, which leads to a warming in the Northern Hemisphere. Pedro et al. (2015)

485 note that the cooling in this ACR simulation induced by the AMOC strengthening at the end of Heinrich Stadial

1 is further amplified by the expansion of Southern Hemisphere sea ice. However, the ACR simulation is also

limited in that it does not capture Older Dryas cooling over the Northern Hemisphere (He, 2011), and the

improved ACR representation without freshwater forcing is difficult to reconcile with sea level records that

indicate the pronounced meltwater discharge of MWP1A (Deschamps et al., 2012).

490   In comparison to TraCE-21ka, the DG_{ns} experiment better matches the duration of the ACR, but shows

more modest temperature changes, particularly over the EAIS interior region. Prescribed Southern Hemisphere

meltwater helps induce the ACR in DG_{ns} by reducing AABW formation, thereby decreasing the southward

oceanic heat transport (Menviel et al., 2011). The longer duration and lower magnitude of meltwater forcing

applied to the Ross and Weddell Seas to represent MWP1A in DG_{ns} likely drives these differences with TraCE-

495 21ka, which shows a shorter and more pronounced ACR. The shutdown of the AMOC at ~13ka associated with

the Younger Dryas and AABW strengthening lead to a significant warming at high southern latitudes in the

DG_{ns} experiment. However, this warming does not continue into the early Holocene (11.5-10 kyr) as indicated

by the Southern Ocean SST proxy compilation. TraCE-21ka similarly does not reproduce the warming through

this interval. Bereiter et al., (2018) suggest that this model-proxy mismatch during the early Holocene is not

500 uncommon among GCMs and intermediate complexity models, and may indicate that the current generation of climate models may underestimate ocean heat uptake or that the understanding of the boundary conditions used for ACR/Younger Dryas climate simulations may be flawed. More specifically, given that the precise timing, magnitudes and locations of MWP1A and MWP1B remain a subject of debate (Bard et al., 2010; Deschamps et al., 2012; Gregoire et al., 2016), yet the prescribed meltwater forcings have significant effects on the climate

505 evolutions in these transient simulations (He, 2011; Menviel et al., 2011), accurate model representation through this interval may remain limited until these meltwater discharge events are better constrained.

One of the larger unknowns of the last deglaciation that is of great consequence to ice sheet model simulations are coastal ocean temperature changes at grounding line depths. This is particularly important for WAIS, as the reverse slope bathymetry of the continental shelf creates a configuration prone to retreat, a process

510 that may be currently impacting some regions (Pritchard et al 2012; Favier, 2014). Although the seafloor geometry likely acted as a first order control on ice sheet retreat of grounded ice in some locations (The RAISED Consortium, 2014; Halberstadt et al., 2016), changes in ocean temperature and warm water intrusions underneath ice shelves can dictate the timing of the retreat. The proxy record offers few constraints on coastal sub-surface ocean temperature changes, but the deglacial climate model simulations do offer some insights. In

515 terms of model differences, the sub-surface glacial ocean of TraCE-21ka is cooler relative to the PI as compared to DG_{ns}, hence significantly more warming occurs during the deglaciation, particularly in the Ross, Amundsen and Bellingshausen Seas. However, both climate models show pronounced sub-surface warming associated with MWP1A, indicating that the event may have resulted in a positive feedback between sea ice, AABW production, and thermal erosion at the ice sheet grounding line, as suggested by previous ice sheet model

520 simulations (Golledge et al., 2014). Additional transient climate simulations of the deglaciation using different GCMs and intermediate complexity models are required to more clearly determine which of these differences and similarities in ocean temperatures are model dependent. Considering the significance but great uncertainty of the prescribed meltwater forcings in these simulations, the incorporation of coupling between GCMs and dynamic ice sheet models is a necessary step to ensure that climatically relevant ice-ocean interactions and

525 feedbacks, such as sub-ice shelf melting and ice berg calving, are adequately reproduced in future transient climate simulations. Marine sediment and coastal ice core reconstructions that can be used to evaluate these climate model performances in terms of coastal ocean circulation and sea ice would also be particularly helpful in better understanding Antarctic climate evolution and ice sheet retreat history during the deglaciation.

530 **5. Summary and Conclusions**

Based on spatial and temporal analysis of two transient climate simulations of the last deglaciation, one using a fully coupled GCM (TraCE-21ka) and one using an intermediate complexity model (LOVECLIM DG_{ns}), we explore the regional aspects of Antarctica's deglacial climate evolution. We also assess climate model

535 performances with regard to model output most relevant to ice sheet model simulations, including surface temperature, surface mass balance, coastal ocean temperatures, and sea ice. The main findings of this study are as follows:

The greatest continental surface temperature warming from the glacial termination (18kyr) to the mid-Holocene (6.5kyr) occurs along coastal margins and, in the case of TraCE-21ka, regions with the greatest

540   decrease in ice surface elevation, suggesting the importance of sea ice-albedo feedbacks and ice sheet dynamics
       in Antarctica's deglacial evolution. The centennial-scale rates of temperature change are reasonable as
       compared to the proxy record.

       Strong discrepancies in modelled accumulation (P-E) are observed in the two climate simulations,
       particularly along the EAIS coast, which are related to the coarser resolution of LOVECLIM compared to
545   CCSM3. Both models struggle to match the ice core accumulation reconstructions at the WDC and EDC sites.
       Accumulation-temperature scaling relationships are also not spatially or temporally uniform, with the coastal
       EAIS and AP showing higher variability in the relationship in the early to mid-Holocene.

       The models show some substantial differences with regard to coastal SST and sub-surface ocean
       temperatures. The TraCE-21ka simulation has a considerably cooler glacial Southern Ocean, and as a result,
550   experiences a greater degree of warming to the mid-Holocene. The model simulations are relatively consistent
       in terms of sea ice coverage and thickness along the Antarctic coast. The exception is the Weddell Sea, in which
       TraCE-21ka shows considerably thicker sea ice. TraCE-21ka also likely overestimates Southern Ocean sea ice
       extent in the glacial state.

       Correlations between Southern Ocean SSTs and Antarctic accumulation weaken in the Holocene,
555   coinciding with the reduction of sea ice coverage and increased variability in accumulation-temperature scaling
       over the coastal regions. The increase in open ocean area may allow for greater variation in moisture sources
       and higher synoptic-scale variability, thereby weakening SST-accumulation relationships. Meanwhile, a
       weakened and more stable Amundsen Sea Low appears to decrease accumulation-temperature scaling over the
       AP. A more detailed moisture budget analysis with an emphasis on tropical teleconnections to the Amundsen
560   Sea Low is required to better understand this climatic shift.

       The greatest model-proxy mismatch occurs with the temperature and accumulation changes associated
       with the ACR and the SST changes associated with the early Holocene ocean warming event, in which the
       models do not adequately capture the precise magnitude and duration of change. These mismatches may result
       from model bias in large-scale ocean circulation, poorly constrained boundary conditions during these time
565   periods, or some combination of the two. In particular, deglacial climate evolution is highly sensitive to the
       timing, magnitude and location of prescribed meltwater forcing during this time interval.

       Given the relatively limited number of transient climate simulations of the deglaciation, it remains
       challenging to assess model skill and identify model-dependent biases in capturing the transient aspects of
       climate, including the factors that impact climate-forced ice sheet model simulations. As such, the community
570   would be well served by additional transient climate simulations using different climate models, the
       incorporation of dynamic ice sheet models in climate simulations, and high-resolution proxy records that can aid
       in climate model assessment.

Acknowledgements

575

We gratefully acknowledge the teams behind the TraCE-21ka and LOVECLIM DG$_{ns}$ experiments for producing
and sharing model output, publicly available via the NCAR Climate Data Gateway and the Asia-Pacific Data
Research Center, respectively. We also thank the Antarctic ice core and marine sediment proxy communities for
the use of their data. Funding for this project was provided by the New Zealand Ministry of Business,
580   Innovation, and Employment Grants through Victoria University of Wellington (15-VUW-131) and GNS

Science (540GCT32). DPL acknowledges support from the Antarctica New Zealand Doctoral Scholarship
program. NG acknowledges support from the Royal Society Te Aparangi under contract VUW1501. LM
acknowledges support from the Australian Research Council grant DE150100107.

585 **References**

Alley, R. The Younger Dryas cold interval as viewed from central Greenland, *Quaternary Science Reviews*, 19, 1-5, 213-226, 2000.

590 Annan, J.D., Hargreaves, J.C. Identification of climatic state with limited proxy data. *Climate of the Past*, 8, 1141–1151, 2012.

Bakker, P., Clark, P.U., Golledge, N.R., Schmittner, A., Weber, M.E. Centennial-scale Holocene climate variations amplified by Antarctic Ice Sheet discharge. *Nature* 541, 72-76, 2017.

595 Bard, E., Hamelin, B., Delanghe-Sabatier, D., Deglacial Meltwater Pulse 1B and Younger Dryas sea levels revisited with boreholes at Tahiti, *Science*, 327, 5970, 2010.

Berger, A. Long-term variations of daily insolation and Quaternary climatic changes, *Journal of the* 600 *Atmospheric Sciences*, 35, 2362-2367, 1978.

Bereiter, B., Shackleton, S., Baggenstos, D., Kawamura, K., Severinghaus, J. Mean global ocean temperatures during the last glacial transition. *Nature*, 553, 39-44, 2018. doi:10.1038/nature25152

605 Braconnot, P., Harrison, S.P., Kageyama, M., Bartlein, P.J., Masson-Delmotte, V., Abe-Ouchi, A., Otto-Bliesner, B., Zhao, Y. Evaluation of climate models using palaeoclimatic data. *Nature climate change*, 2, 417–424, 2012.

Brovkin, V., Ganopolski, A., Svirezhev, Y. A continuous climate-vegetation classification for use in climate-610 biosphere studies. *Ecol. Modell*, 101, 251-261, 1997.

Calvo, E., Pelejero, C., Deckker, P.D., Logan, G. Antarctic deglacial pattern in a 30 kyr record of sea surface temperature offshore South Australia. *Geophys. Res. Lett.*, 34, 2007. doi:10.1029/2007GL029937.

615 Campin, J., Goosse, H. Parameterization of density-driven downsloping flow for a coarse-resolution ocean model in z-coordinate. *Tellus*, 51A, 412-430, 1999.

Collins, W.D., *et al.*, The Community Climate System Model Version 3 (CCSM3), *Journal of Climate*, 19, 2122-2143, 2006.

620 Cuffey, K.M., G.D. Clow, E.J. Steig, C. Buizert, T.J. Fudge, M. Koutnik, E.D. Waddington, R.B. Alley, and J.P. Severinghaus. Deglacial temperature history of West Antarctica. *Proc. Natl. Acad. Sci.* 113(50): 14249-14254, 2016. doi:10.1073/pnas.1609132113.

Denton, G.H., Anderson, R.F., Toggweiler, J.R., Edwards, R.L., Schaefer, J.M., Putnam, A.E. The Last Glacial Termination. *Science*, 328, 1652-1656, 2010.
625
Delaygue, G, Masson, V., Jouzel, J., Koster, R.D., Healy, R.J. The origin of Antarctic precipitation: a modelling approach, *Tellus* 52B, 19–3, 2000.

Deschamps, P., Durand, N., Bard, E. Hamelin, B., Camoin, G., Thomas, A.L., Henderson, G.M., Okuno, J., 630 Yokoyama, Y. Ice-sheet collapse and sea-level rise at the Bølling warming 14,600 years ago, *Nature,* 483, 559–564, 2012.

Driesschaert, E., Fichefet, T., Goosse, H., Huybrechts, P., Janssens, I., Mouchet, A., Munhoven, G., Brovkin, V., Weber, S.L., Modeling the influence of Greenland ice sheet melting on the Atlantic meridional overturning 635 circulation during the next millennia, *Geophysical Research Letters*, 34, 10, 2007.

Favier, L., Durand, G., Cornford, S.L., Gudmundsson, G.H., Gagliardini, O., Gillet-Chaulet, F., Zwinger, T., Payne, A.J., Le Brocq, A.M. Retreat of Pine Island Glacier controlled by marine ice-sheet instability. *Nature Climate Change* 4, 117-121, 2014.

Frieler, K., Clark, P.U., He, F., Buizert, C., Reese, R., Ligtenberg, S.R.M., van den Broeke, M.R., Winkelmann, R., Levermann, A. Consistent evidence of increasing Antarctic accumulation with warming. *Nature Climate Change*, 5, 348-352, 2015. doi:10.1038/NCLIMATE2574

Fudge, T.J., Markle, B.R., Cuffey, K.M., Buizert, C., Taylor, K.C., Steig, E.J., Waddington, E.D., Conway, H., Koutnik, M. Variable relationship between accumulation and temperature in West Antarctica for the past 31,000 years, *Geophysical Research Letters* 43, 3795–3803, 2016.

Genthon, G., J. M. Barnola, D. Raynaud, C. Lorius, J. Jouzel, N. I. Barkov, Y. S. Korotkevich, and V. M. Kotlyakov, Vostok ice core: climatic response to CO2 and orbital forcing changes over the last climatic cycle, *Nature*, 329 (6138), 414-418, 1987.

Gersonde, R., Crosta, X., Ableman, A., Armand, L. Sea-surface temperature and sea ice distribution of the Southern Ocean at the EPILOG Last Glacial Maximum—a circum-Antarctic view based on siliceous microfossil records, *Quaternary Science Reviews*, 24, 869–896, 2005.

Golledge, N.R., Menviel, L., Carter, L., Fogwill, C.J., England, M.H., Cortese, G., Levy, R.H. Antarctic Contribution to meltwater pulse 1A from reduced Southern Ocean overturning. *Nature Communications* 5, 5107, 2014.

Golledge, N.R., Levy, R.H., McKay, R.M., Naish, T.R. East Antarctic ice sheet most vulnerable to Weddell Sea warming. *Geophysical Research Letters*, 2017.

Goosse, H., Driesschaert, E., Fichefet, T., Loutre, M.-F. Information on the early Holocene climate constrains the summer sea ice projections for the 21st century. *Climate of the Past*, 3, 4, 683-692, 2007.

Goosse, H., Brovkin, V., Fichefet, T., Haarsma, R., Huybrechts, P.,Jongma, J., Mouchet, A., Selten, F., Barriat, P.-Y., Campin, J.-M., Deleersnijder, E., Driesschaert, E., Goelzer, H., Janssens, I., Loutre, M.-F., Morales Maqueda, M. A., Opsteegh, T., Mathieu, P.-P., Munhoven, G., Pettersson, E. J., Renssen, H., Roche, D. M., Schaeffer, M., Tartinville, B., Timmermann, A., and Weber, S. L.: Description of the Earth system model of intermediate complexity LOVECLIM version 1.2, *Geosci. Model Dev.*, 3, 603–633, 2010. doi:10.5194/gmd-3-603-2010

Goose, H., Mairesse, A., Mathiot, P., Philippon, G., Antarctic temperature changes during the last millennium: evaluation of simulations and reconstructions. *Quaternary Science Reviews*, 55, 75-90, 2012.

Gregoire, L.J., Otto-Bleisner, B., Valdes, P.J., Ivanovic, R. Abrupt Bølling warming and ice saddle collapse contributions to the Meltwater Pulse 1a rapid sea level rise. *Geophysical Research Letters*, 43, 9130-9137, 2016. doi:10.1002/2016GL070356.

Haargreaves, J.C., Annan, J.D., Ohgaito, R., Paul, A., Abe-Ouchi, A. Skill and reliability of climate model ensembles at the Last Glacial Maximum and mid-Holocene. *Climate of the Past*, 9, 811–823, 2013.

Halberstadt, A.R.W., Simkins, L.M., Greenwood, S.L., Anderson, J.B. Past ice-sheet behavior: retreat scenarios and changing controls in the Ross Sea, Antarctica. *The Cryosphere*, 10, 1003-1020, 2016. doi:10.5194/tc-10-1003-2016

He, F. TraCE-21ka: Simulation of Transient Climate Evolution over the last 21,000 years. Ph.D. dissertation, University of Wisconsin, Madison, 2011.

He, F., J. D. Shakun, P. U. Clark, A. E. Carlson, Z. Liu, B. L. Otto-Bliesner, and J. E. Kutzbach (2013), Northern Hemisphere forcing of Southern Hemisphere climate during the last deglaciation, *Nature*, 494, 7435, 81-85, 2013.

640

645

650

655

660

665

670

675

680

685

690

695   Hosking, J. S., Orr, A., Marshall, G.J, Turner, J., Phillips, T. The influence of the Amundsen–Bellingshausen
      Seas low on the climate of West Antarctica and its representation in coupled climate model simulations. *Journal
      of Climate*, 26, 6633–6648, 2013. doi:10.1175/JCLI-D-12-00813.1.

      Jones, T.R., Roberts, W.H.G., Steig, E.J., Cuffey, K.M., Markle, B.R., White, J.W.C. Southern Hemisphere
700   climate variability forced by Northern Hemisphere ice-sheet topography. *Nature*, 554, 351-355, 2018.
      doi:10.1038/nature24669.

      Joos, F., Spahni, R. Rates of change in natural and anthropogenic radiative forcing over the past 20,000 years,
      PNAS, 105 (5) 1425-1430, 2008. 10.1073/pnas.0707386105

705
      Jouzel, J., *et al.,* Validity of the temperature reconstruction from water isotopes in ice cores, *J. Geophys. Res.*,
      102, 26, 471–26, 487, 1997. doi:10.1029/97JC01283.

      Jouzel, J., V. Masson-Delmotte, O. Cattani, G. Dreyfus, S. Falourd, G. Hoffmann, B. Minster, J. Nouet, J.M.
710   Barnola, J. Chappellaz, H. Fischer, J.C. Gallet, S. Johnsen, M. Leuenberger, L. Loulergue, D. Luethi, H. Oerter,
      F. Parrenin, G. Raisbeck, D. Raynaud, A. Schilt, J. Schwander, E. Selmo, R. Souchez, R. Spahni, B. Stauffer,
      J.P. Steffensen, B. Stenni, T.F. Stocker, J.L. Tison, M. Werner, and E.W. Wolff. 2007. Orbital and Millennial
      Antarctic Climate Variability over the Past 800,000 Years. *Science*, 317, 5839, 793-797, 2007.

715   Kaiser, J., Lamy, F., Hebbeln, D. A 70-kyr sea surface temperature record off Southern Chile.
      Paleoceanography, 20, 2005. doi:10.1029/2004PA001146.

      Levis, S., Bonan, G.B., Vertenstein, M., Oleson, K.W. The Community Land Model's Dynamic Global
      Vegetation Model (CLM-DGVM): Technical description and user's guide. Tech. Rep. NCAR/TN-459+IA,
720   National Center for Atmospheric Research, Boulder, CO, 2004.

      Liu, Z., Otto-Bleisner, B.L., He, F., Brady, E.C., Tomas, R., Clark, P.U., Carlson, A.E., Lynch-Stieglitz, J.,
      Curry, W., Brook, E., Erickson, D., Jacob, R., Kutzbach, J., Cheng, J. Transient Simulation of Last Deglaciation
      with a New Mechanism for Bølling-Allerød Warming. *Science* 325, 310-314, 2009.

725
      Lorius, C., J. Jouzel, C. Ritz, L. Merlivat, N.I. Barkov, Y.S. Korotkevitch, and V.M. Kotlyakov. A 150,000-year
      climatic record from Antarctic ice. *Nature*, 316:591-596, 1995.

      McKay, R., Golledge, N.R., Maas, S., Naish, T., Levy, R., Dunbar, G., Kuhn, G. Antarctic marine ice-sheet
730   retreat in the Ross Sea during the early Holocene. *Geology* 1, 7-10, 2016.

      McManus, J.F., Francois, R., Gherardi, J.M., Keigwin, L.D., Brown-Leger, S. Collapse and rapid resumption of
      Atlantic meridional circulation linked to deglacial climate changes. *Nature*, 428, 834-837, 2004.

735   Medley, B., *et al.,* Airborne-radar and ice-core observations of annual snow accumulation over Thwaites
      Glacier, West Antarctica confirm the spatiotemporal variability of global and regional atmospheric models.
      Geophysical Research Letters, 40, 3649–3654, 2013. doi:10.1002/grl.50706

      Menviel, L., Timmermann, A., Elison Timm, O., Mouchet, A. Climate and biogeochemical response to a rapid
740   melting of the West-Antarctic Ice Sheet during interglacials and implications for future climate,
      Paleoceanography, 25, PA4231, 2010. doi:10.1029/2009PA001892.

      Menviel, L., Timmermann, A., Timm, O.E., Mourchet, A. Deconstructing the Last Glacial termination: the role
      of millennial and orbital-scale forcings. *Quaternary Science Reviews* 30, 1155-1172, 2011.

745
      Menviel, L., Timmerman, A., Friedrich, T., England, M.H. Hindcasting the continuum of Dansgaard–Oeschger
      variability: mechanisms, patterns and timing. *Climate of the Past*, 10, 63–77, 2014.

      Monnin, E., *et al.*, Atmospheric CO_2 Concentrations over the Last Glacial Termination, *Science*, 290, 5501, 112-
750   114, 2001.

      Monnin, E., Steig, E.J., Siegenthaler, U., Kawamura, K., Schwander, J., Stauffer, B., Stocker, T.F., Morse, D.L.,
      Barnola, J.M., Blandine, B., Raynaud, D., Fischer, H. Evidence for substantial accumulation rate variability in

755   Antarctica during the Holocene, through synchronization of CO_2 in the Taylor Dome, Dome C and DML ice cores, *Earth and Planetary Science Letters*, 224, 45–54, 2004.

Mouchet, A., Francois, L. Sensitivity of a Global Oceanic Carbon Cycle Model to the circulation and to the fate of organic matter: preliminary results. *Phys. Chem. Earth*, 21, 511-516, 1996.

760   Mulvaney, R., Abram, N.J., Hindmarsh, R.C.A., Arrowsmith, C., Fleet, L., Triest, J., Sime, L.C., Alemany, O., Foord, S. Recent Antarctic Peninsula warming relative to Holocene climate and ice-shelf history. *Nature*, 489, 7414, 141-144, 2012. DOI: 10.1038/nature11391

Opsteegh, J., Haarsma, R., Selten, F., Kattenberg, A. ECBILT: a dynamic alternative to mixed boundary
765   conditions in ocean models. *Tellus*, 50A, 348-367, 1998.

Palerme, C., Genthon, C., Claud, C., Kay, J.E., Wood, N.B., L'Ecuyer, T. Evaluation of current and projected Antarctic precipitation in CMIP5 models, *Climate Dynamics*, 48, 225-239, 2017. doi:10.1007/s00382-016-3071-1.
770
Pahnke, K., Zahn, R., Elderfield, H., Schulz, M. 340,000-year centennial-scale marine record of Southern Hemisphere climatic oscillation. *Science* 301, 948-952, 2003.
Palm, S.P., Kayetha, V., Yang, Y., Pauly, R. Blowing snow sublimation and transport over Antarctica from 11 years of CALIPSO observations. *The Cryosphere*, 11, 2555-2569, 2017. doi: 10.5194/tc-11-2555-2017
775
Parrenin, F., *et al.*, The EDC3 chronology for the EPICA Dome C ice core. *Climate of the Past*, 3, 485-497, 2007.

Pedro, J.B., van Ommen, T.D., Rasmussen, S.O., Morgan, V.I., Chappellaz, J., Moy, A.D., Masson-Delmotte,
780   V., Delmotte, M. The last deglaciation: timing the bipolar seesaw. *Climate of the Past*, 7, 671–683, 2011. doi:10.5194/cp-7-671-2011

Pedro, J.B., Bostock, H.C., Bitz, C.M., He, F., Vandergoes, M.J., Steig, E.J., Chase, B.M., Krause, C.E., Rasmussen, S.O., Markle, B.R., Cortese, G. The spatial extent and dynamics of the Antarctic Cold Reversal,
785   *Nature Geoscience*, 9, 51-55, 2015. doi:10.1038/NGEO2580.

Peltier, W. Ice-age paleotopography. *Science* 265, 195-201, 1994.

Peltier, W. R. Global glacial isostasy and the surface of the ice-age Earth- The ICE-5 G(VM 2) model and
790   GRACE, *Annu. Rev. Earth Planet. Sci*., 32 (1), 111-149, 2004.

Petit, J.R., J. Jouzel, D. Raynaud, N.I. Barkov, J.M. Barnola, I. Basile, M. Bender, J. Chappellaz, J. Davis, G. Delaygue, M. Delmotte, V.M. Kotlyakov, M. Legrand, V. Lipenkov, C. Lorius, L. Pépin, C. Ritz, E. Saltzman, and M. Stievenard. Climate and atmospheric history of the past 420,000 years from the Vostok Ice Core,
795   Antarctica. *Nature*, 399:429-436, 1999.

Pollard, D., DeConto, R.M. Modelling West Antarctic ice sheet growth and collapse through the past five million years. *Nature*, 458, 329–332, 2009.

800   Pritchard, H.D., Ligtenberg, S.R.M., Fricker, H.A., Vaughan, D.G., van den Broeke, M.R., Padman, L. Antarctic ice-sheet loss driven by basal melting of ice shelves. *Nature* 484, 502-505, 2012.

The RAISED consortium, *et al.,* A community-based geological reconstruction of Antarctic ice sheet deglaciation since the Last Glacial Maximum. *Quaternary Science Reviews*, 100, 1-9, 2014.
805   Uemura, R., V. Masson-Delmotte, J. Jouzel, A. Landais, H. Motoyama, and B. Stenni. Ranges of moisture-source temperature estimated from Antarctic ice cores stable isotope records over glacial-interglacial cycles. *Climate of the Past*, 8, 1109-1125, 2012. doi: 10.5194/cp-8-1109-2012

Raphael, M.N., Marshall, G.J., Turner, J., Fogt, R.L., Schneider, D., Dixon, D.A., Hosking, J.S., Jones, J.M.,
810   Hobbs, W.R. The Amundsen Sea Low: Variability, change, and impact on Antarctic Climate, *Bulletin of the American Meteorological Society*, 97, 111-121, 2016. doi:10.1175/BAMS-D-14-00018.1.

Sachs, J.P., Anderson, R.F., Lehman, S.J. Glacial Surface Temperatures of the Southeast Atlantic Ocean. *Science*, 293, 2077 - 2079, 2001.

815

Schmidt, G.A., *et al.,* Climate forcing reconstructions for use in PMIP simulations of the Last Millennium (v1.1). *Geosci. Model Dev.,* 5, 185–191, 2012. doi:10.5194/gmd-5-185-2012

Stenni, B., Masson-Delmotte, V., Selmo, E., Oerter, H., Meyer, H., Röthlisberger, R., Jouzel, J., Cattani, O.,
820   Falourd, S., Fischer, H., Hoffmann, G., Iacumin, P., Johnsen, S.J., Minster, B., Udisti, R. The deuterium excess records of EPICA Dome C and Dronning Maud Land ice cores (East Antarctica). *Quaternary Science Reviews*, 29, 146-159, 2010.

Sueyoshi, T., *et al.,* Set-up of the PMIP3 paleoclimate experiments conducted using an Earth system model,
825   MIROC-ESM. *Geosci. Model Dev.,* 6, 819–836, 2013. doi:10.5194/gmd-6-819-2013

Timmermann, A., Menviel, L., Okumura, Y., Schilla, A., Merkel, U., Timm, O., Hu, A., Otto-Bleisner, B., Schulz, M. Towards a quantitative understanding of millennial-scale Antarctic warming events, *Quaternary Science Reviews* 29, 74–85, 2010.
830
Veres, D., *et al.,* The Antarctic ice core chronology (AICC2012): an optimized multi-parameter and multi-site dating approach for the last 120 thousand years. *Climate of the Past*, 9, 1733–1748, 2013. doi:10.5194/cp-9-1733-2013

835   WAIS Divide Project Members, Onset of deglacial warming in West Antarctica driven by local orbital forcing. *Nature*, 500, 440-444, 2013.

840

845

850

855

860

865

870

Figures & Tables

Table 1. Model details and specifications.

875

Model Simulation	Atmosphere Component	Land Component	Ocean Component	Sea Ice component
TraCE-21ka	Community Atmospheric Model 3 (CAM3) (Collins et al., 2006) 3.75° horizontal resolution, 26 hybrid coordinate vertical resolution	Community Land Model-Dynamic Global Vegetation Module (CLM-DGVM) (Levis et al. 2004) 3.75° horizontal resolution	Parallel Ocean Program (POP) (Collins et al., 2006) vertical z-coordinate with 25 levels, 3.6° longitudinal resolution, and variable latitudinal resolution, with finer resolution near the equator (~0.9°)	Community Sea Ice Model (CSIM) (Collins et al., 2006) Thermodynamic/ dynamic model that includes sub-grid ice thickness distribution 3.6° longitudinal and variable latitudinal resolution, with finer resolution near the equator (~0.9°)
LOVECLIM DG_ns	ECBilt (Opsteegh et al., 1998) quasi-geostrophic T21 spectral, 3 levels	VECODE (Brovkin et al., 1997) dynamic vegetation module	CLIO (Campin and Goose, 1999) primitive equations, z-coordinate, 3 x 3 resolution model with 20 levels LOCH (Mouchet and Francois, 1996) 3-dimensional ocean carbon cycle model	Thermodynamic/ dynamic sea ice model coupled to CLIO

880

885

890

895

900

Table 2. Antarctic and Southern Ocean proxy record details.

Record name	Type	Measurement	Method	Location	Reference
Vostok (V)	Ice core	Temperature anomaly	δD temperature calibration	East Antarctica, 78.5°S, 107°E	Lorius et al., 1995; Petit et al., 1999
Dome Fuji (DF)	Ice core	Temperature anomaly	*d* temperature calibration	East Antarctica, 77°S, 39°E	Uemura et al., 2012
James Ross Island (JRI)	Ice core	Temperature anomaly	δD temperature calibration	Antarctic Peninsula, 64°S, 58°W	Mulvaney et al., 2012
EPICA Dome C (EDC)	Ice core	Temperature anomaly; Accumulation	δD temperature calibration; Ice flow model	East Antarctica, 75°S, 124°E	Jouzel et al., 2007; Parennin et al., 2007; Stenni et al., 2010
WAIS Divide (WDC)	Ice core	Surface temperature; Accumulation	Water stable isotope record; borehole temperatures and nitrogen isotopes; Ice flow model	West Antarctica, 79.5°S, 112°W	WAIS Divide Project Members, 2013; Cuffey et al., 2016; Fudge et al., 2016
Core MD03-2611	Marine sediment core	SST	Alkenone-derived	Murray Canyons area, 36°S, 136°E	Calvo et al., 2007
ODP site 1233 core	Marine sediment core	SST	Alkenone-derived	SE Pacific, 41°S, 74°W	Kaiser et al., 2005
Core MD97-2120	Marine sediment core	SST	Mg/Ca-derived	Chatham Rise, 45°S, 175°E	Pankhe et al., 2003
Core TN057-21-PC2	Marine sediment core	SST	Alkenone-derived	South Atlantic, 41°S, 8°E	Sachs et al., 2001

905
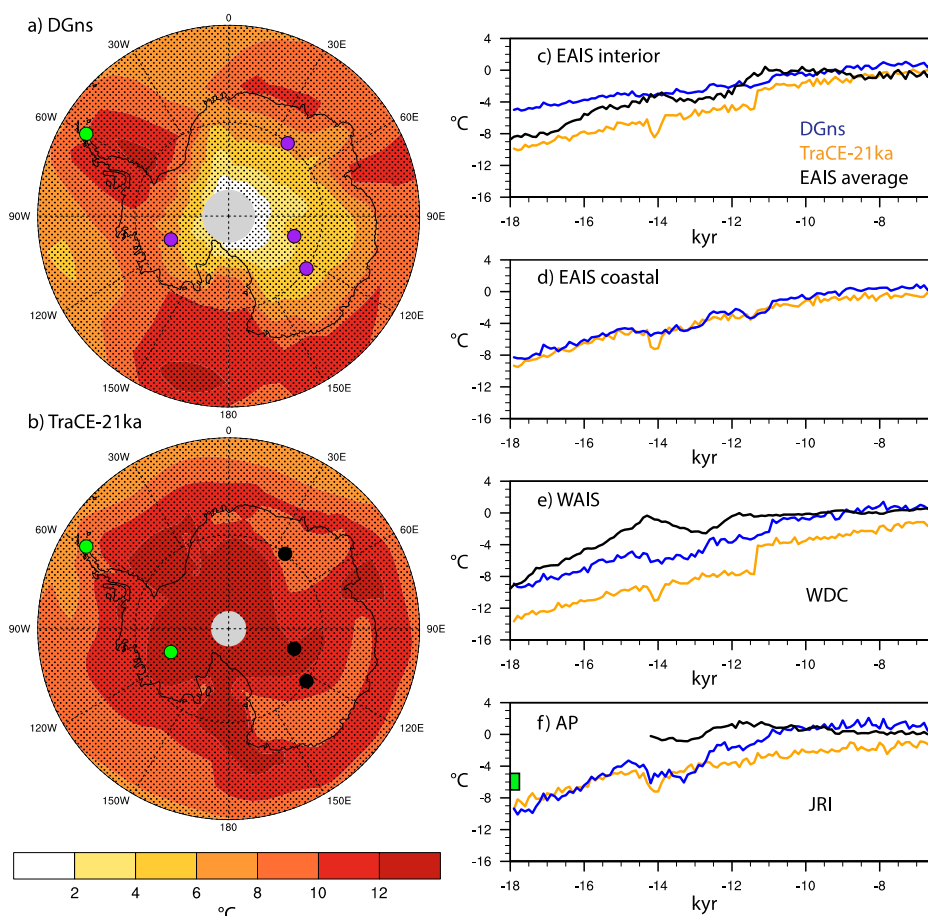
Figure 1: Surface temperature warming (°C) as simulated in (a) DG$_{ns}$ and (b) TraCE-21ka for the period of 18 to 6.5 kyr. Ice core locations of the JRI, WDC, DF, V, and EDC sites are marked by filled circles, with black circles indicating a match in warming between the ice core and model simulation (within the range of proxy temperature reconstruction uncertainty of -10% to +30%), and green (purple) circles indicating an overestimation (underestimation) in warming by the models. For these model-proxy comparisons, we use site-specific model averages of land surface grid cells: JRI (63-65°S, 59-62°W), WDC (77-82°S, 115-109°W), DF (75-79°S, 36-42°E), V (77-82°S, 104-110°E), EDC (73-77°S, 121-127°E). Stippling indicates a difference between decadal output of 18.0-17.5 kyr and 7.0-6.5 kyr that is significant at the 95% confidence level. (c-e) 100-yr average surface temperature time series (°C) of four regions (EAIS interior: 83°S-75°S, 30°W-165°E; coastal EAIS: 75°S-68°S, 15°W-165°E; WAIS: 83°S-72°S, 165°E-30°W; AP: 72°S-64°S, 64°W-59°W) relative to PI of both model simulations and ice core temperature reconstructions of sites located therein (DG$_{ns}$ in blue, TraCE-21ka in orange, ice cores in black). For EAIS, the ice core reconstruction is an average of the DF, V and EDC sites. The green box in (f) indicates the LGM temperature anomaly estimated for JRI (6.01±1.0°C; Mulvaney et al., 2012).
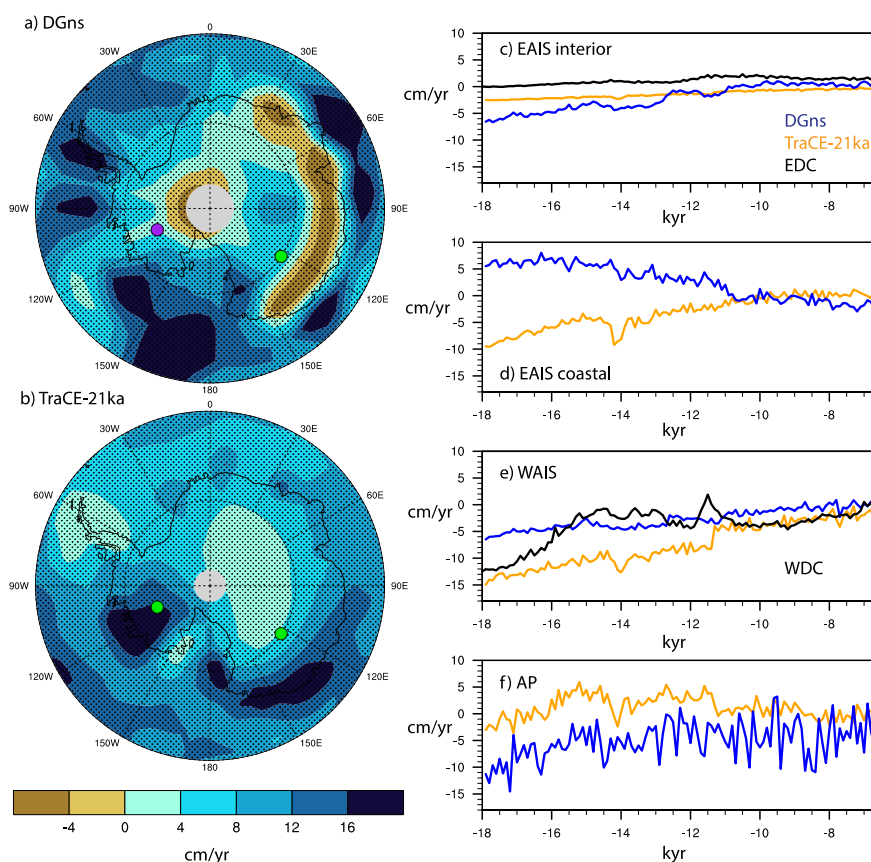
Figure 2: Precipitation change (cm/yr) as simulated in (a) DG$_{ns}$ and (b) TraCE-21ka for the period of 18 to 6.5 kyr. Ice core locations of WDC and EDC are marked by the filled circles, with black circles indicating a match between the modelled precipitation change and ice core accumulation (within the range of proxy uncertainty of ±20%), and green (purple) circles indicating an overestimation (underestimation) in precipitation change by the models. For these model-proxy comparisons, we use site-specific model averages of land surface grid cells: WDC (77-82°S, 115-109°W), EDC (73-77°S, 121-127°E). Stippling indicates a difference between decadal output of 18.0-17.5 kyr and 7.0-6.5 kyr that is significant at the 95% confidence level. (c-e) 100-yr average accumulation time series (cm/yr) of four regions (EAIS interior: 83°S-75°S, 30°W-165°E; coastal EAIS: 75°S-68°S, 15°W-165°E; WAIS: 83°S-72°S, 165°E-30°W; AP: 72°S-64°S, 64°W-59°W) relative to PI of both model simulations (P-E) and ice core accumulation reconstructions of sites located therein (DG$_{ns}$ in blue, TraCE-21ka in orange, ice cores in black).
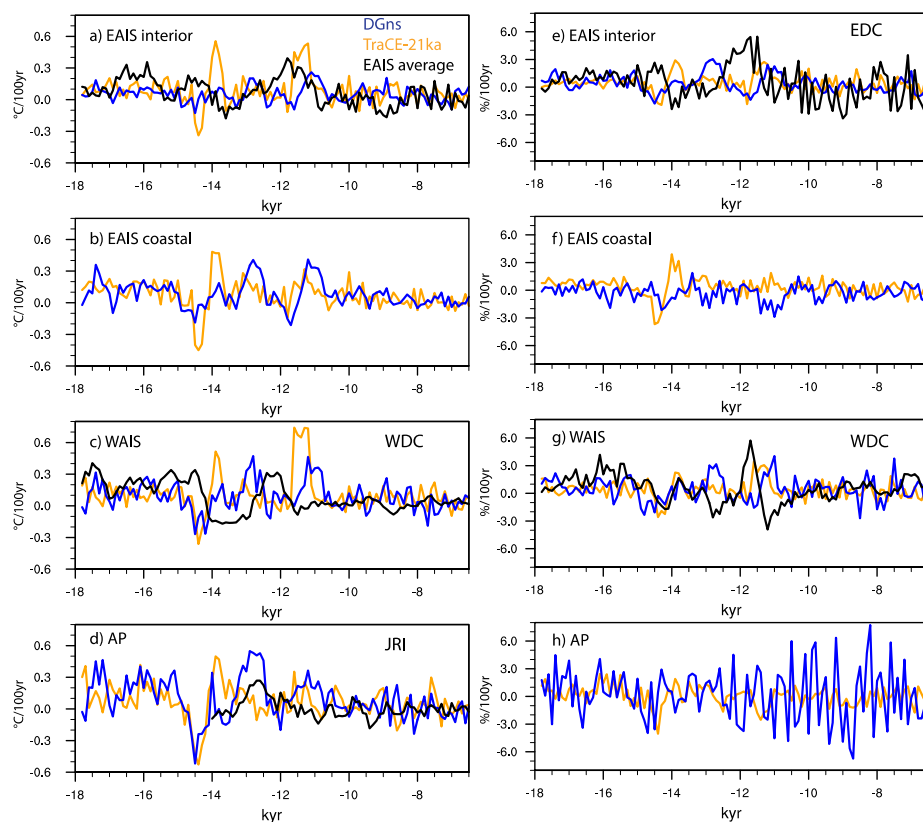
935

Figure 3: Centennial-scale rates of (a-d) surface temperature change (°C) and (e-h) relative accumulation change (%; DG$_{ns}$ in blue, TraCE-21ka in orange, ice cores in black).
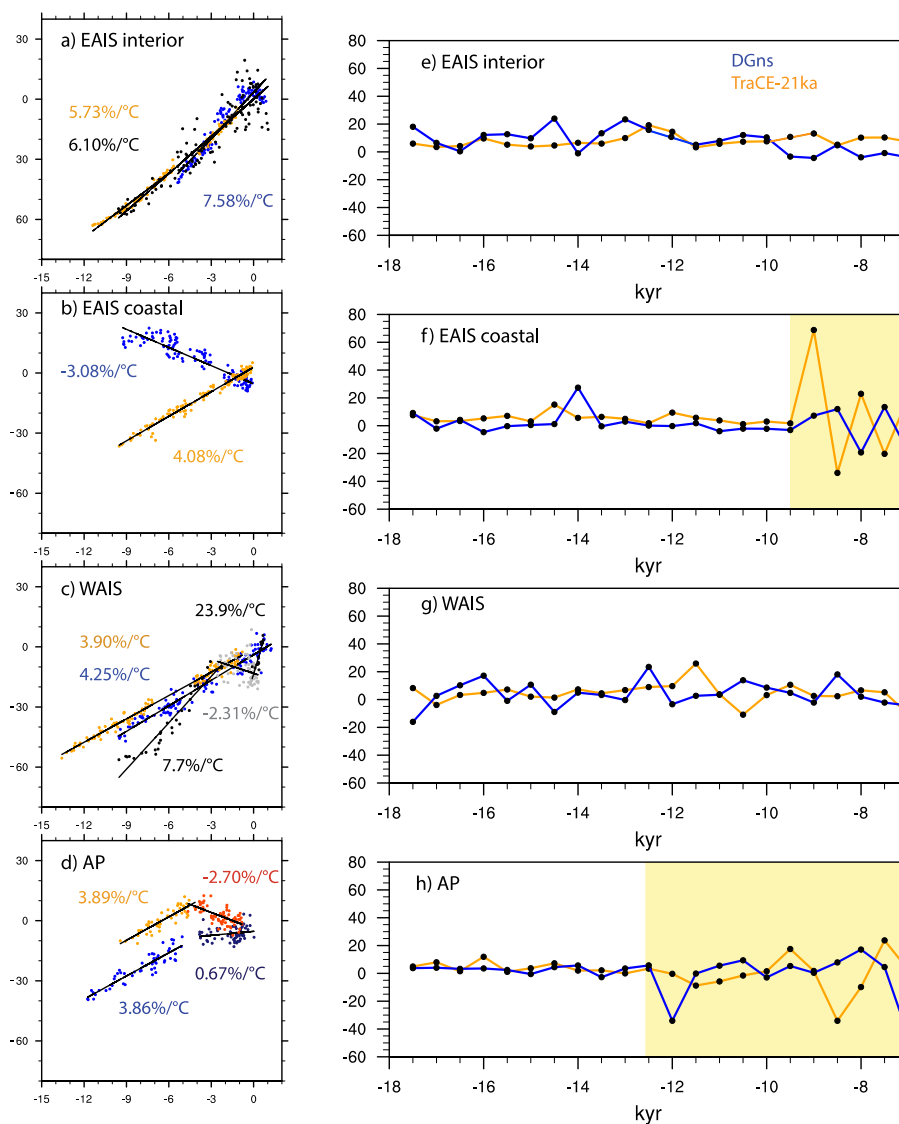
940

Figure 4: (a-d) Scaling relationships of accumulation and temperature in each region. Black and grey dots refer to the proxy record, blue and purple dots refer to the DG_{ns} simulation, and orange and red dots refer to the TraCE21ka simulation. (e-h) The ratio of the change in precipitation (%) to the change in temperature (°C) per 500 years.
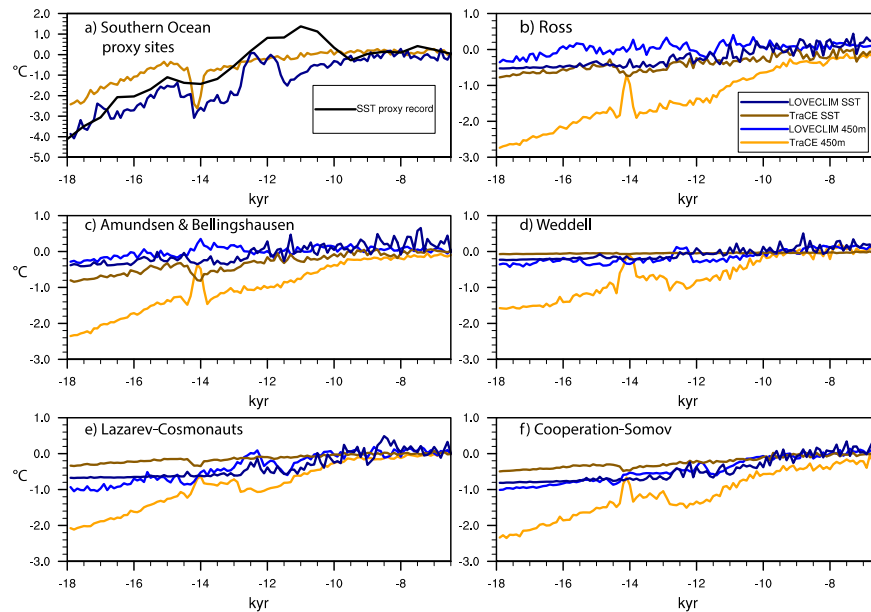
945

Figure 5: Time series of 100-yr average SST and 450 m depth ocean temperature of the coastal seas around Antarctica, namely, the Ross Sea (70°S—62°S, 168°E—160°W), the Amundsen and Bellingshausen Seas (68°S—62°S, 135°W—60°W), the Weddell Sea (70°S—62°S, 60°W—30°W), the coastal region from Lazarev

950   Sea to Cosmonauts Seas (67°S—62°S, 15°W—50°E), and the coastal region from Cooperation Sea to Somov Sea (67°S—62°S, 55°E—165°E).
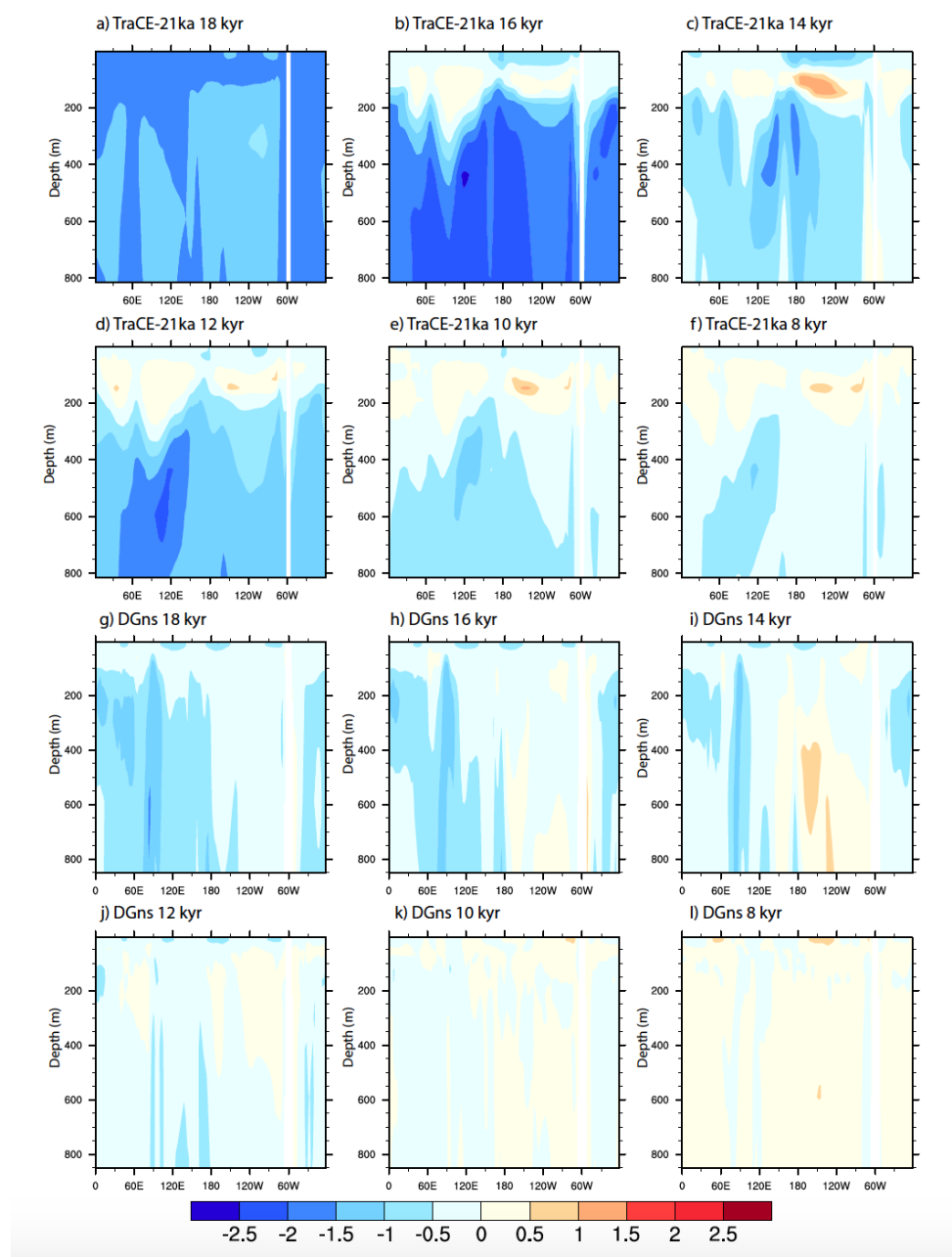
Figure 6: 2-kyr time slices of longitudinal cross-sections of 100 yr-averaged ocean temperature anomalies
relative to PI at 64°S the surface to 800 m depth: (a-f) TraCE-21ka 18kyr to 8 kyr; (g-l) DG$_{ns}$ 18kyr to 8kyr.
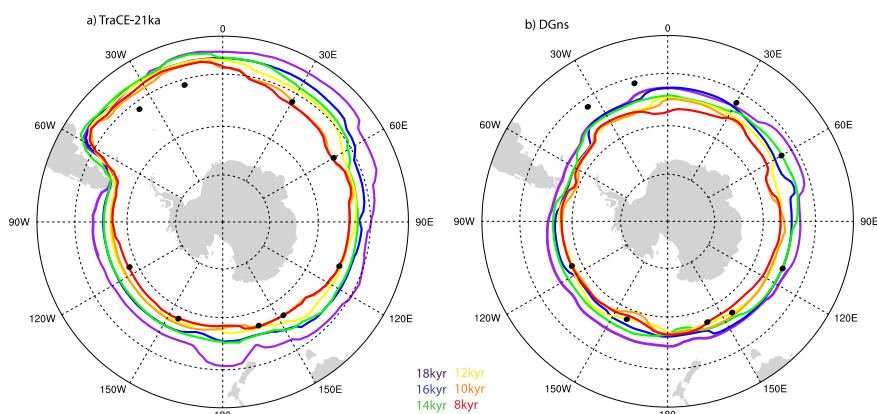
Figure 7: Modelled sea ice extent (5% coverage contour) per 2-kyr for (a) TraCE-21ka and (b) DG$_{ns}$ from 18-8 kyr. The black dots indicate LGM limits from the proxy record (adapted from Gersonde et al., 2005; we include the lowest latitude points >5%).
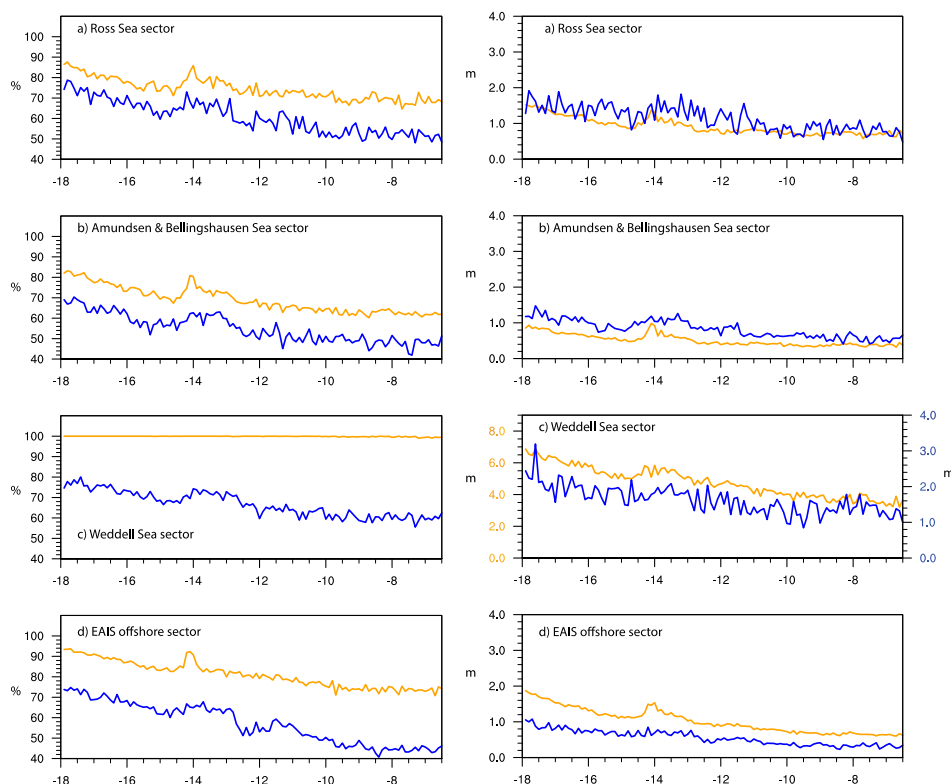
Figure 8: Time series of 100-yr average (a-d) sea ice thickness (m) and (e-h) coverage (%) in the Southern
Ocean, namely, the Ross Sea sector (70°S—50°S, 168°E—160°W), the Amundsen and Bellinghausen Sea
965   sector (68°S—50°S, 135°W—60°W), the Weddell Sea sector (70°S—50°S, 60°W—30°W), and the offshore
EAIS sector from Lazarev Sea to Somov Sea (67°S—50°S, 15°W—165°E).
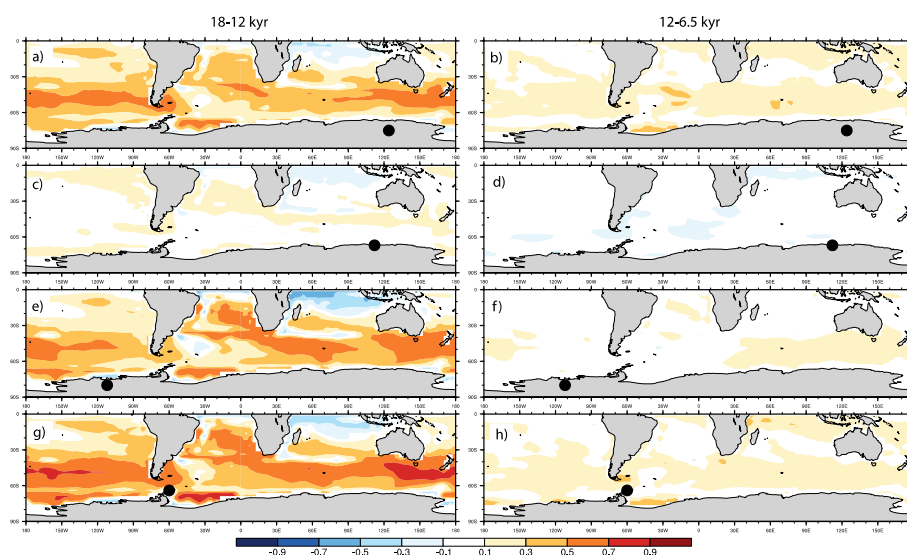
Figure 9: Spatial Pearson linear cross-correlation coefficients (r) between de-trended decadal SST and
precipitation of the DG$_{ns}$ simulation for (left) 18-12 kyr and (right) 12-6.5 kyr at the (a,b) EDC (73-77°S, 121-
127°E), (c,d) LD (65-70°S, 110-116°E), (e,f) WDC (77-82°S, 115-109°W), and (g,h) JRI (63-65°S, 59-62°W)
ice core locations, respectively.
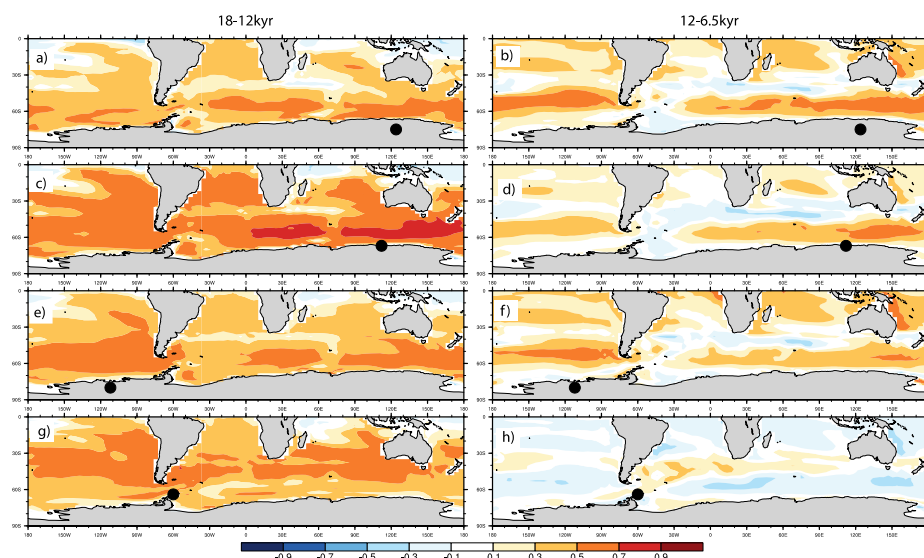
980

Figure 10: Spatial Pearson linear cross-correlation coefficients (r) between de-trended decadal SST and precipitation of the TraCE-21ka for (left) 18-12 kyr and (right) 12-6.5 kyr at the (a,b) EDC (73-77°S, 121-127°E), (c,d) LD (65-70°S, 110-116°E), (e,f) WDC (77-82°S, 115-109°W), and (g,h) JRI (63-65°S, 59-62°W) ice core locations, respectively.
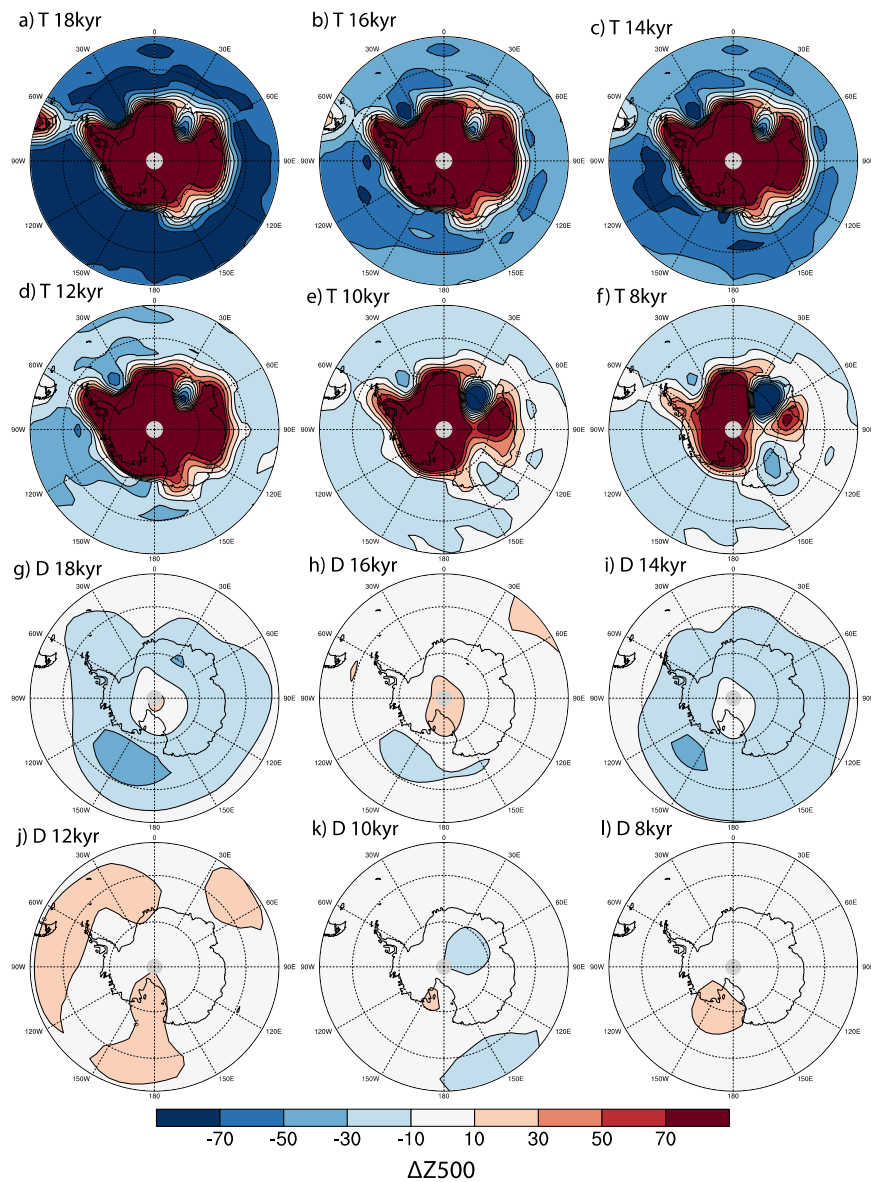
985

Figure 11: Geopotential height anomalies (m) at 500hPa relative to PI for the (a-f) TraCE-21ka and (g-l) DG$_{ns}$
deglacial experiments.

990